Kusmierek, J. T., & Singer, B. (1982) *Biochemistry 21*, 5717-5722.
Laib, R. J., & Bolt, H. M. (1977) *Toxicology 8*, 185-195.
Laib, R. J., Gwinner, L. M., & Bolt, H. M. (1981) *Chem.-Biol. Interact. 37*, 219-231.
Leonard, N. J. (1984) *CRC Crit. Rev. Biochem. 15*, 125-199.
Osterman-Golkar, S., Hultmark, D., Segerback, D., Calleman, C. J., Gothe, R., Ehrenberg, L., & Wachtmeister, C. A. (1977) *Biochem. Biophys. Res. Commun. 76*, 259-266.
Sattsangi, P. D., Leonard, N. J., & Frihart, C. R. (1977) *J. Org. Chem. 42*, 3292-3296.
Scherer, E., Van Der Laken, C. J., Gwinner, L. M., Laib, R. J., & Emmelot, P. (1981) *Carcinogenesis 2*, 671-677.
Secrist, J. A., III, Barrie, J. R., Leonard, N. J., & Weber, G. (1972) *Biochemistry 11*, 3499.
Singer, B., & Grunberger, D. (1983) *Molecular Biology of Mutagens and Carcinogens*, Plenum Press, New York.
Singer, B., & Bartsch, H., Eds. (1986) *The Role of Cyclic Nucleic Acid Adducts in Carcinogenesis and Mutagenesis*, IARC Scientific Publications 70, IARC, Lyon, France.
Singer, B., & Spengler, S. J. (1986) in *The Role of Cyclic Nucleic Acid Adducts in Carcinogenesis and Mutagenesis* (Singer, B., & Bartsch, H., Eds.) IARC Scientific Publications 70, pp 359-371, IARC, Lyon, France.
Singer, B., Abbott, L. G., & Spengler, S. J. (1984) *Carcinogenesis 5*, 1165-1171.
Singer, B., Spengler, S. J., Chavez, F., & Kusmierek, J. T. (1987) *Carcinogenesis 8*, 745-747.
Spengler, S., & Singer, B. (1981) *Nucleic Acids Res. 9*, 365-373.

NMR Studies of the Exocyclic 1,N^6-Ethenodeoxyadenosine Adduct (ϵdA) opposite Deoxyguanosine in a DNA Duplex. ϵdA(syn)·dG(anti) Pairing at the Lesion Site†

Carlos de los Santos,‡ Michael Kouchakdjian,‡ Kevin Yarema,§ Ashis Basu,§ John Essigmann,*,§ and Dinshaw J. Patel*,‡

Department of Biochemistry and Molecular Biophysics, College of Physicians and Surgeons, Columbia University, New York, New York 10032, and Department of Chemistry and Whitaker College of Health Sciences and Technology, Massachusetts Institute of Technology, Cambridge, Massachusetts 02139

Received September 6, 1990; Revised Manuscript Received October 29, 1990

ABSTRACT: Proton NMR studies are reported on the complementary d(C-A-T-G-G-G-T-A-C)·d(G-T-A-C-ϵA-C-A-T-G) nonanucleotide duplex (designated ϵdA·dG 9-mer duplex), which contains the exocyclic adduct 1,N^6-ethenodeoxyadenosine positioned opposite deoxyguanosine in the center of the helix. The present study focuses on the alignment of dG5 and ϵdA14 at the lesion site in the ϵdA·dG 9-mer duplex at neutral pH. This alignment has been characterized by monitoring the NOEs originating from the NH1 proton of dG5 and the H2, H5, and H7/H8 protons of ϵdA14 in the central d(G4-G5-G6)·d(C13-ϵA14-C15) trinucleotide segment of the ϵdA·dG 9-mer duplex. These NOE patterns establish that ϵdA14 adopts a syn glycosidic torsion angle that positions the exocyclic ring toward the major groove edge while all the other bases including dG5 adopt anti glycosidic torsion angles. We detect a set of intra- and interstrand NOEs between protons (exchangeable and nonexchangeable) on adjacent residues in the d(G4-G5-G6)·d(C13-ϵA14-C15) trinucleotide segment which establish formation of right-handed helical conformations on both strands and stacking of the dG5(anti)·ϵdA14(syn) pair between stable dG4·dC15 and dG6·dC13 pairs. The energy-minimized conformation of the central d(G4-G5-G6)·d(C13-ϵA14-C15) segment establishes that the dG5(anti)·ϵdA14(syn) alignment is stabilized by two hydrogen bonds from the NH1 and NH_2-2 of dG5(anti) to N9 and N1 of ϵdA14(syn), respectively. The NH1 proton of dG5 resonates at 14.0 ppm, and its downfield shift is consistent with hydrogen bond formation with the ring nitrogen (N9) of ϵdA14 at the lesion site in the ϵdA·dG 9-mer duplex. The H6 and H5 base protons of dC13 and dC15 are broad in the ϵdA·dG 9-mer duplex, with some broadening also observed at the H2 and H5 base protons of ϵdA14 in NMR spectra recorded at ambient temperature. The observed broadening may originate in conformational averaging among ϵdA14 alignments on the intermediate time scale, which would affect the stacking in the d(C13-ϵA14-C15) segment centered about the lesion site. In summary, the dG5(anti)·ϵdA14(syn) alignment is readily accommodated into the DNA helix without disruption of flanking dG4·dC15 and dG6·dC13 base pairs and may account for the incorporation of dG opposite ϵdA during in vitro replication by DNA polymerase I.

There is currently very little known at the molecular level about structural features of nucleic acid exocyclic adducts important in mutagenesis and carcinogenesis (Singer & Bartsch, 1986). The formation of these adducts not only interferes with base pairing regions of nucleic acid components but also induces substantial alterations in the pK_a and hydrophobicity at the lesion site. There is a potential for local helix distortion at exocyclic adduct sites with important consequences on polymerase fidelity and repair efficiency at the lesion site.

Our groups are collaborating on an investigation of the structure and base pairing alignments of the 1,N^6-ethenodeoxyadenosine (ϵdA) exocyclic adduct **1** incorporated in DNA

†This research was supported by NIH Grant CA-49982 to D.J.P. and NIH Grant CA-52127 to J.E. C.d.l.S. was supported by an NIH International Fogarty Fellowship.
‡Columbia University.
§Massachusetts Institute of Technology.

0006-2960/91/0430-1828$02.50/0

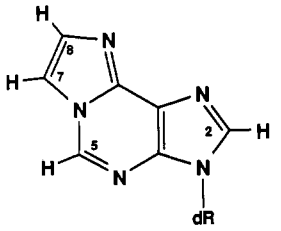

1

oligomer duplexes in an attempt to correlate molecular structure with biological function. The previous paper focused on an NMR study of the ϵdA adduct positioned opposite dT in the center of a complementary deoxynonanucleotide duplex (Kouchakdjian et al., 1991). This paper extends these studies to the ϵdA adduct positioned opposite dG within the same sequence context in the d(C1-A2-T3-G4-G5-G6-T7-A8-C9)·d(G10-T11-A12-C13-ϵA14-C15-A16-T17-G18) duplex (**2**). Previously, it has been demonstrated from in vitro rep-

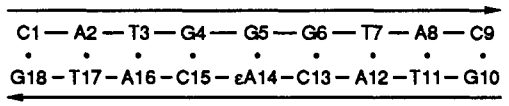

2

lication studies that deoxyguanosine is misincorporated in synthetic poly(dA) or poly(dA-dT) templates and natural DNAs treated with chloroacetaldehyde (Barbin et al., 1981; Hall et al., 1981; Singer et al., 1984). Furthermore, recent genetic studies have shown that ϵdA can induce A → C transversions in vivo (Basu and Essigmann, manuscript in preparation).

Experimental Procedures

Oligodeoxynucleotide Synthesis. The synthesis of the ϵdA14-modified strand is reported in the preceding paper (Kouchakdjian et al., 1991). The unmodified strand was synthesized on a 10-μmol scale using phosphoramidite chemistry on a Beckman System 1 plus automated DNA synthesizer. The isolation, deprotection, and purification procedures have been reported previously (de los Santos et al., 1989).

Sample Preparation. A 1:1 stoichiometry of the ϵdA·dG 9-mer duplex was achieved at 42 °C by monitoring the intensities of the deoxyadenosine base resonances and thymidine methyl resonances during the gradual addition of the unmodified strand to the lesion-containing strand. The NMR experiments were performed on samples containing 290 A_{260} units of the ϵdA·dG 9-mer duplex dissolved in 0.4 mL of 20 mM phosphate buffer (pH 6.8) containing 50 mM NaCl and 0.5 mM EDTA in either 100% D_2O or 90% H_2O/10% D_2O (v/v). The pH values in D_2O are uncorrected pH meter readings.

NMR Experiments. Proton NMR experiments were performed at either 400 or 500 MHz on Bruker AM series spectrometers. Proton chemical shifts were referenced relative to 3-(trimethylsilyl)propionate-*2,2,3,3-d*$_4$ (TSP). Pulse sequence, data acquisition, and processing parameters for the two-dimensional NOESY experiments in H_2O were similar to those reported previously (de los Santos et al., 1989).

Two-dimensional phase-sensitive (States et al., 1982) NOESY spectra (250-, 100-, and 50-ms mixing times) in D_2O were recorded by using quadrature detection, and the residual water signal was presaturated with a continuous-wave radio frequency during the relaxation and mixing times. Time domain data sets consisted of 1024 complex points in the t_2 dimension and 256 increments in the t_1 dimension. The free

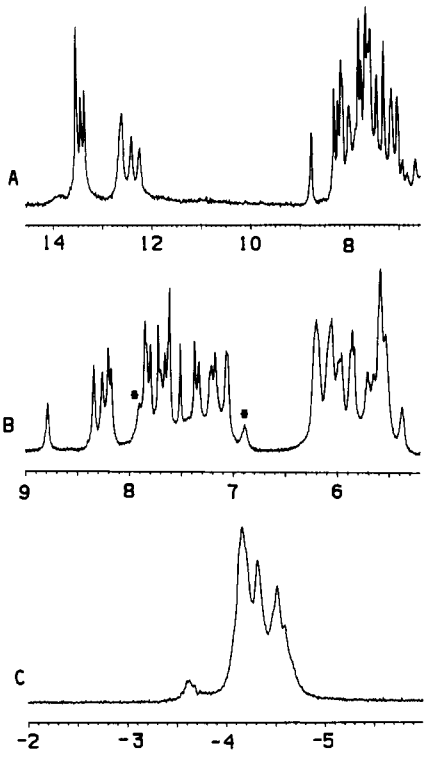

FIGURE 1: (A) Exchangeable proton (6.0–15.0 ppm), (B) nonexchangeable proton (5.2–9.0 ppm), and (C) proton-decoupled phosphorus (−2 to −6 ppm) spectra of the ϵdA·dG 9-mer duplex in 0.1 M NaCl and 10 mM phosphate, aqueous solution, pH 6.8, at 10, 18, and 13 °C, respectively.

induction decays were apodized by using a 90°-shifted sine bell function zeroed to the 1024th point in the t_2 dimension before Fourier transformation. The spectra in the t_2 dimension were base line corrected with a fifth-order polynomial base-line fitting routine. COSY experiments were recorded in the magnitude mode. All data sets were processed by using FTNMR software on either a VAX 6310 or a micro VAXII minicomputer.

Energy Minimization. Volume integrals of the NOE cross peaks at 50- and 100-msec mixing times were used to estimate the interproton distance constraints in the ϵdA·dG 9-mer duplex. Canonical B-form DNA starting structures were constructed by using the program MacroModel. Deoxyadenosine at position 14 was modified to introduce the etheno bridge. Further, the glycosidic torsion angle at position ϵdA14 was changed from the anti to the syn range as defined by the experimental data. Two starting structures with different values for the ϵdA14 glycosidic torsion angle in the syn range were energy minimized by using the XPLOR program on a CONVEX C220 minisupercomputer. The minimization parameters were the same as those used in the preceding paper (Kouchakdjian et al., 1991).

Results

The ϵdA·dG 9-mer duplex **2** exhibits well-resolved exchangeable proton (6.5–14.5 ppm) (Figure 1A) and nonexchangeable proton (5.0–9.0 ppm) (Figure 1B) spectra at pH 6.8 so that structural features of the solution conformation can be characterized by two-dimensional NMR methods.

Exchangeable Protons. Exchangeable proton NMR spectra of the ϵdA·dG 9-mer duplex in 0.1 M NaCl, 10 mM phosphate, and H_2O, pH 6.8, as a function of temperature between 18 and −4 °C are plotted in Figure S1 (supplementary material). The ϵdA·dG 9-mer duplex spectrum exhibits an exchangeable proton resonance at 14.0 ppm at −4 °C, which

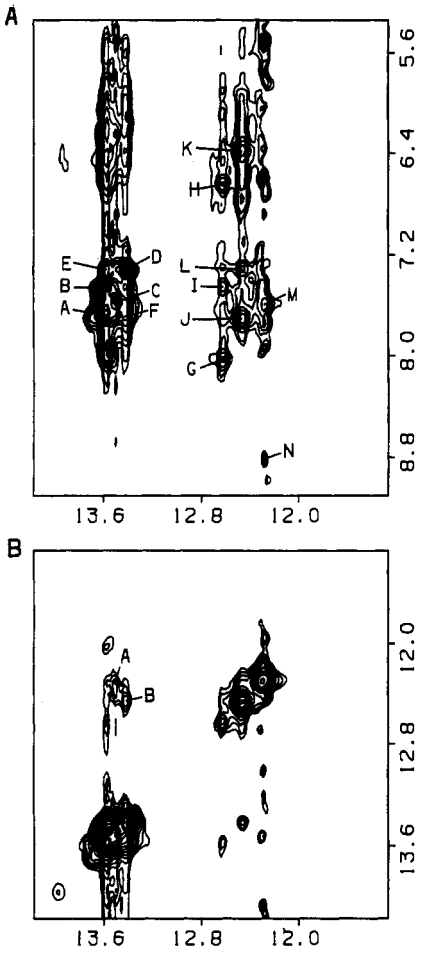

FIGURE 2: Expanded contour plots of the NOESY spectrum (mixing time 150 ms) of the ϵdA·dG 9-mer duplex in 0.1 M NaCl and 10 mM phosphate H_2O, pH 6.8 at 2 °C. (A) NOE cross peaks establishing connectivities between the 11.5–14.0 ppm imino proton region and the 5.5–8.2 ppm base and amino proton region. Cross peaks A–N are assigned as follows: A, T17(NH3)–A2(H2); B, T11(NH3)–A8(H2); C, T3(NH3)–A16(H2); D, T7(NH3)–A12(H2); E, T11-(NH3)–A12(H2); F, T7(NH3)–C13(NH4b); G, G10(NH1)–C9-(NH4b); H, G10(NH1)–C9(NH4e); I, G10(NH1)–A8(H2); J, G6(NH1)–C13(NH4b); K, G6(NH1)–C13(NH4e); L, G6-(NH1)–A12(H2); M, G4(NH1)–A16(H2); N, G4(NH1)–ϵA14(H5). (B) NOE cross peaks establishing connectivities in the symmetrical 11.5–14.0 ppm imino proton region. Cross peaks are assigned as follows: A, T3(NH3)–G4(NH1); B, T7(NH3)–G6(NH1).

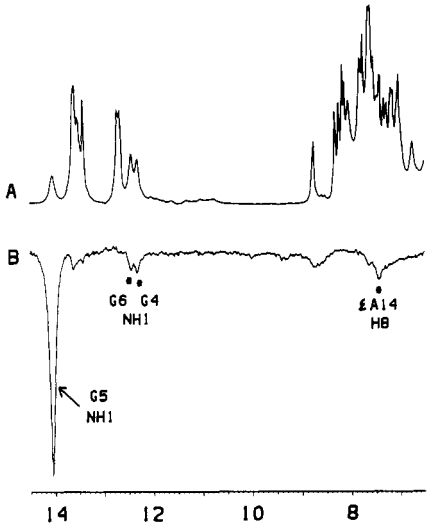

FIGURE 3: (A) Exchangeable proton spectrum (6.0–15.0 ppm) of the ϵdA·dG 9-mer duplex in 0.1 M NaCl and 10 mM phosphate, H_2O, pH 6.8 at −6 °C. (B) One-dimensional NOE diffrence spectrum following 0.5-s saturation of the 14.04 ppm resonance.

broadens significantly on raising the temperature to 18 °C. In addition, the imino protons of the terminal dC1·dG18 and dC9·dG10 base pairs at ~12.6 ppm broaden with increasing temperature (Figure S1).

The imino protons in the ϵdA·dG 9-mer duplex have been assigned following analysis of NOESY data sets recorded in H_2O buffer, pH 6.8, at 2 and 10 °C. Expanded NOESY contour plots of the 150-ms mixing time NOESY spectrum at 2 °C establishing connectivities between the imino protons (11.5–14.1 ppm) and the amino and nonexchangeable protons (5.5–8.2 ppm) are plotted in Figure 2A, and those establishing connectivities in the symmetrical 11.5–14.1 ppm imino proton region are plotted in Figure 2B. We detect NOE cross peaks between the thymidine imino protons and deoxyadenosine H2 protons (peaks A–D, Figure 2A) for the four dA·dT pairs in the ϵdA·dG 9-mer duplex. The thymidine imino protons can be assigned to the dA2·dT17, dT3·dA16, dT7·dA12, and dA8·dT11 base pairs on the basis of an independent assignment of deoxyadenosine H2 protons in the ϵdA·dG 9-mer duplex. We detect an NOE (peak A, Figure 2B) between the 13.49 ppm imino proton of the dT3·dA16 base pair and the 12.28 ppm imino proton that must be assigned to the adjacent dG4·dC15 base pair. Similarly, an NOE (peak B, Figure 2B) is detected between the 13.41 ppm imino proton of the dT7·dA12 base pair and the 12.46 ppm imino proton that must be assigned to the adjacent dG6·dC13 base pair in the ϵdA·dG 9-mer duplex.

The 12.46 ppm dG6 imino proton exhibits NOEs to hydrogen-bonded and exposed amino protons of deoxycytidine (peaks J and K, Figure 2A) within the dG6·dC13 pair and an NOE to the H2 proton of dA12 (peak L, Figure 2A) of the flanking dT7·dA12 pair. By contrast, we do not detect NOEs between the 12.28 ppm dG4 imino proton and the amino protons of dC15, suggesting that these amino protons may be broad in the ϵdA·dG 9-mer duplex. The dG4 imino proton of the dG4·dC15 base pair does exhibit NOEs to the H2 proton of dA16 (peak M, Figure 2A) of the flanking dT3·dA16 pair and the 8.81 ppm H5 proton of ϵdA14 (peak N, Figure 2A) of the flanking dG5·ϵdA14 lesion site in the ϵdA·dG 9-mer duplex.

The low-field 14.04 ppm exchangeable proton did not exhibit NOE cross peaks in the 150-ms mixing time NOESY spectrum of the ϵdA·dG 9-mer duplex in H_2O, pH 6.8 at 2 °C. This observation presumably reflects the rapid exchange of this proton, which competes effectively with magnetization transfer during the mixing time of the NOESY experiment. We therefore recorded one-dimensional NOE difference spectra on the ϵdA·dG 9-mer duplex in H_2O buffer, pH 6.8 at −6 °C, with the difference spectrum following 0.5-s saturation of the 14.04 ppm exchangeable resonance plotted in Figure 3B. We detect NOEs at the imino protons of dG4 and dG6, establishing that the 14.04 ppm exchangeable resonance can be assigned to the imino proton of dG5 at the dG5·ϵdA14 lesion site. Saturation of the 14.04 ppm imino proton of dG5 also exhibits an NOE at the 7.41 ppm H7/H8 protons of ϵdA14 within the dG5·ϵdA14 lesion site in the ϵdA·dG 9-mer duplex (Figure 3B).

The chemical shifts of the imino and amino exchangeable protons and the deoxyadenosine H2 protons in the ϵdA·dG 9-mer duplex in H_2O buffer, pH 6.8, 2 °C, are listed in Table I.

Nonexchangeable Protons. The nonexchangeable base and sugar protons have been assigned following analysis of the 250-ms mixing time NOESY contour plot of the ϵdA·dG

Table I: Proton Chemical Shifts in the ϵdA·dG 9-mer Duplex[a]

	chemical shift (ppm)			
base pair	T(NH3)	G(NH1)	C(NH_2-4)[b]	A(H2)
C1·G18		12.63	8.04, 6.91	
A2·T17	13.57			7.67
T3·A16	13.49			7.57
G4·C15		12.28	nd[c]	
G5·ϵA14		14.04		
G6·C13		12.46	7.71, 6.38	
T7·A12	13.41			7.32
A8·T11	13.56			7.45
C9·G10		12.62	8.03, 6.64	

[a] 50 mM NaCl, 10 mM phosphate, H_2O, pH 6.8. [b] Hydrogen-bonded deoxycytidine amino proton downfield from exposed deoxycytidine amino proton. [c] nd, not detected.

9-mer duplex in D_2O buffer, pH 6.8 at 18 °C (Figure S2A, supplementary material). The NOE cross peaks are well resolved as can be seen in the duplicate expanded contour plot connecting the base protons (6.8–8.9 ppm) with the sugar H1′ protons (5.1–6.4 ppm) (Figure 4). The NOE connectivities between the base protons and their own and 5′-flanking sugar H1′ protons can be traced from dC1 to dC9 without interruption in the unmodified strand in Figure 4A. By contrast, the base to sugar H1′ NOE connectivities from dG10 to dG18 on the modified strand are interrupted at the dC13-ϵdA14 step in the ϵdA·dG 9-mer duplex (Figure 4B). We detect a strong but broad NOE cross peak between the H2 of ϵdA14 and its own sugar H1′ proton (peak labeled dA14, Figure 4B) with an intensity approaching that of the H6–H5 protons of deoxycytidines in 250-ms mixing time, as well as 50-ms mixing time, NOESY data sets (Figure S2B, supplementary material). The H2 proton of ϵdA14 exhibits no detectable cross peak to the sugar H1′ of its 5′-flanking dC13 and a weak cross peak to the sugar H1′ of its 3′-flanking dC15 (peak B, Figure 4B) neighbor. The strong NOE between the H2 and H1′ protons of ϵdA14 establishes a syn glycosidic torsion angle at the modified base in the ϵdA·dG 9-mer duplex in solution.

The NOE between the H6 and H5 protons (fixed separation of 2.45 Å) of dC13 is weak and that of dC15 is either very weak or absent in the 50-ms mixing time NOESY spectra of the ϵdA·dG 9-mer duplex (Figure S2B). This suggests that the H6 and H5 protons of dC15 in the dG4·dC15 pair and to a lesser extent of dC13 in the dG6·dC13 pair are broadened as a result of conformational averaging of the alignment at the flanking dG5·ϵdA14 lesion site in the ϵdA·dG 9-mer duplex.

The expanded 250-ms NOESY contour plot connecting the base protons (6.8–8.9 ppm) with the sugar H2′,2″ protons (1.2–3.2 ppm) in the ϵdA·dG 9-mer duplex is plotted in Figure 5A. Each base proton exhibits NOEs to its own and 5′-flanking sugar H2′,2″ protons with some exceptions. Specifically, the only NOE from the H2 proton of ϵdA14 is a weak one to its own H2″ proton (peak C, Figure 5A) and must reflect the syn glycosidic torsion angle at ϵdA14 in the ϵdA·dG 9-mer duplex.

The broadening of the H6 protons of dC13 and dC15 results in weak NOE cross peaks to their own and 5′-flanking sugar H1′ protons (Figure 4B) and H2′,2″ protons (Figure 5A). By contrast, the sugar H1′ to H2′,2″ NOE cross peaks for dC13 and dC15 are normal indicating that motional averaging at the dG5·ϵdA14 lesion site does not affect the line widths of the sugar protons of flanking dC13 and dC15 in the ϵdA·dG 9-mer duplex.

NOE cross peaks were observed between the 8.81 ppm H5 proton and the superpositioned 7.48 ppm H7 and H8 (peak A, Figure 5B) protons of ϵdA14 in the ϵdA·dG 9-mer duplex. Further, the H5 proton of ϵdA14 exhibits NOEs to the H1′ (peak A, Figure 4A), H2′ (peak A, Figure 5A), H2″ (peak B, Figure 5A), and H3′ protons of dC13 in the dC13-ϵdA14 step in the ϵdA·dG 9-mer duplex.

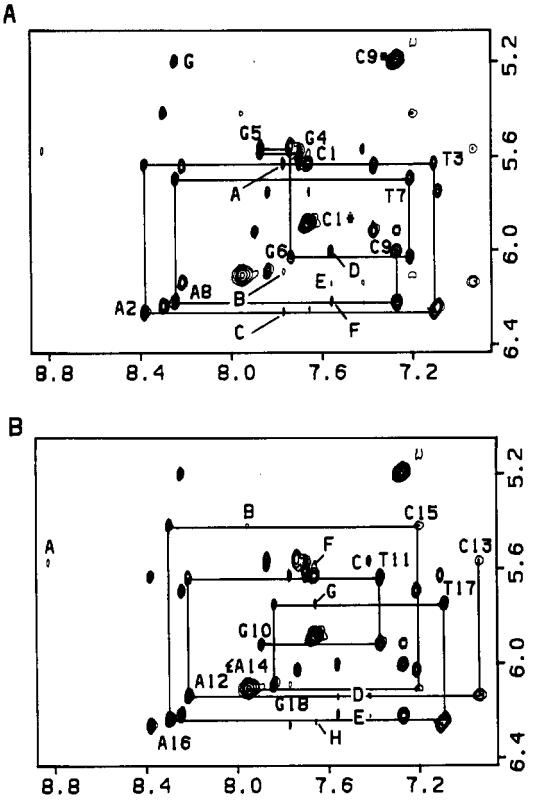

FIGURE 4: Expanded duplicate contour plots of the NOESY spectrum (250-ms mixing time) of the ϵdA·dG 9-mer duplex in 0.1 M NaCl and 10 mM phosphate, D_2O, pH 6.8 at 18 °C. This region establishes distance connectivities between the base protons (6.8–8.9 ppm) and the sugar H1′ and deoxycytidine H5 protons (4.6–6.4 ppm). (A) The chain is traced from dC1 to dC9 on the unmodified strand. The tracing follows connectivities between adjacent base protons through their intervening sugar H1′ protons. The deoxycytidine H5–H6 cross peaks are designated by asterisks. Cross peaks A–F are assigned as follows: A, A2(H2)–T3(H1′); B, A2(H2)–G18(H1′); C, A2(H2)–A2(H1′); D, A8(H2)–C9(H1′); E, A8(H2)–A12(H1′); F, A8(H2)–A8(H1′); G, A8(H8)–C9(H5). (B) The chain is traced from dG10 to dG18 in the modified strand. Cross peaks A–H are assigned as follows: A, ϵA14(H5)–C13(H1′); B, ϵA14(H2)–C15(H1′); C, A12(H2)–C13(H1′); D, A12(H2)–A12(H1′); E, A12(H2)–A8(H1′); F, A16-(H2)–G4(H1′); G, A16(H2)–T17(H1′); H, A16(H2)–A16(H1′).

We have observed NOEs between purine H8 and pyrimidine H5/CH_3 protons in the purine (3′–5′) pyrimidine dA8-dC9 (peak G, Figure 4A), dA2-dT3 (peak D, Figure 5A), dG6-dT7 (peak G, Figure 5A), dG10-dT11 (peak F, Figure 5A), and dA16-dT17 (peak E, Figure 5A) steps in the ϵdA·dG 9-mer duplex. These NOEs are characteristic of a right-handed duplex at purine(3′–5′)pyrimidine steps. By contrast, no NOE was detected between the H2 proton of ϵdA14 and the H5 proton of dC15 in the ϵdA14-dC15 step due to either the syn glycosidic torsion angle at ϵdA14 and/or the broad line width of the H5 proton of dC15 in the ϵdA·dG 9-mer duplex.

Each minor groove H2 proton of deoxyadenosine should exhibit NOEs to the H1′ protons of its own sugar, the adjacent sugar in the 3′-direction on the same strand, and the adjacent sugar in the 5′-direction on the partner strand for a right-handed DNA duplex. We observe these cross peaks to the assigned sugar H1′ protons from the H2 protons of dA2 (peaks A–C, Figure 4A), dA8 (peaks D–F, Figure 4A), dA12 (peaks C–E, Figure 4B), and dA16 (peaks F–H, Figure 4B), providing an independent assignment of the deoxyadenosine H2 protons in the ϵdA·dG 9-mer duplex.

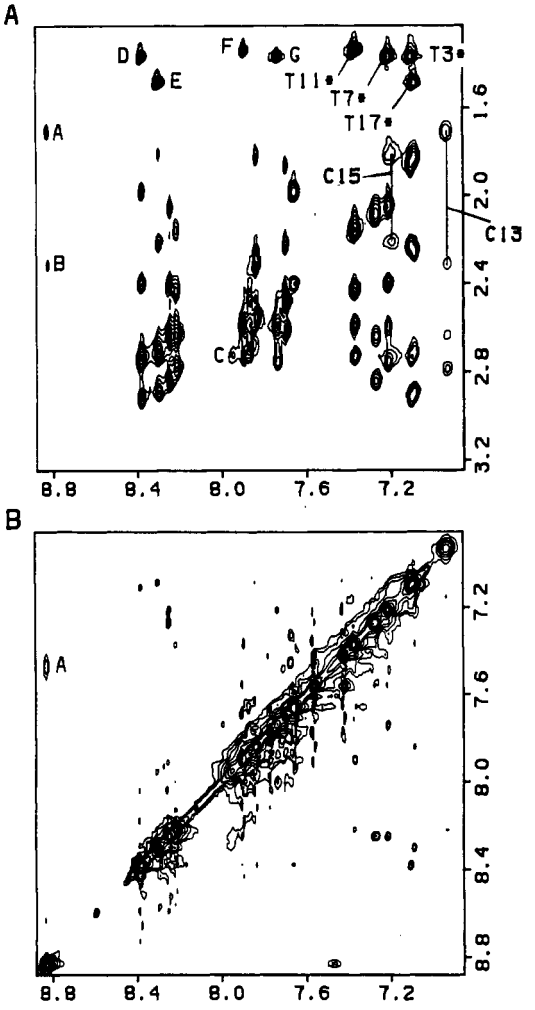

FIGURE 5: Expanded contour plots of the NOESY spectrum (250-ms mixing time) of the ϵdA·dG 9-mer duplex in 0.1 M NaCl and 10 mM phosphate, D_2O, pH 6.8 at 18 °C. (A) This region establishes distance connectivities between the base protons (6.8–8.9 ppm) and the sugar H2′,2″ protons (1.2–3.2 ppm) region. NOE cross peaks A–G are assigned as follows: A, ϵA14(H5)–C13(H2′); B, ϵA14(H5)–C13-(H2″); C, ϵA14(H2)–A14(H2″); D, A2(H8)–T3(CH_3-5); E, A16-(H8)–T17(CH_3-5); F, G10(H8)–T11(CH_3-5); G, G5(H8)–T7-(CH_3-5). The thymidine H6-CH_3 cross peaks are designated by asterisks. (B) This region establishes distance connectivities in the symmetrical 6.8–8.9 ppm base proton region. A, ϵA14(H5)–ϵA14-(H7).

The base and sugar proton chemical shift assignments in the ϵdA·dG 9-mer duplex at 18 °C are listed in Table II, and these values are based on an analysis of the entire NOESY spectrum (Figure S2A) and COSY spectrum.

Phosphorus Spectra. The proton-decoupled phosphorus spectrum of the ϵdA·dG 9-mer duplex in D_2O, pH 6.8 at 13 °C, is plotted in Figure 1C. The phosphorus spectrum is broad, with resonances dispersed between −3.5 and −4.5 ppm. This limited resolution has prevented assignment of the phosphorus resonances in the ϵdA·dG 9-mer duplex at the current time.

Energy Minimization. A total of 124 distance constraints defined by lower and upper bounds were estimated from the volume integrals of the resolved and assigned NOE cross peaks in 50- and 100-ms mixing time NOESY spectra of the ϵdA·dG 9-mer duplex. These were incorporated as square-well potential constraints in the energy minimization algorithm of the XPLOR program. The bounds were tighter for distances estimated from NOESY data sets at mixing times of 50 ms compared to 100 ms. The estimated distances were given lower and upper bounds of −0.5 and +0.6 Å for the NOESY data set collected at a mixing time of 50 ms and lower and upper bounds of −0.6 and +1.0 Å for the NOESY data set collected at a mixing time of 100 ms. We did not incorporate hydrogen-bond constraints for dG5·ϵdA14 alignment at the lesion site, nor was a hydrogen bond constraint included between the O6 of dG4 and the NH_2-4 of dC15 along the major groove edge of the dG4·dC15 pair. The NOE distance constraints defined by lower and upper bounds for the central d(G4-G5-G6)·d(C13-ϵA14-C15) trimer segment of the ϵdA·dG 9-mer duplex are listed in Table III.

The two starting structures had the glycosidic torsion angles (O4′–C1′–N1–C4) of ϵdA14 at either extreme of the syn conformational range (70° and 100°). Close contacts between dG5 and ϵdA14 at the lesion site in the starting structures were

Table II: Nonexchangeable Proton Chemical Shifts in the ϵdA·dG 9-mer Duplex at 18 °C[a]

	chemical shift (ppm)							
base	H8	H2	H6	H5/Me	H1′	H2′	H2″	H3′
C1			7.66	5.89	5.63	1.99	2.40	4.69
A2	8.38	7.77			6.26	2.74	2.92	5.01
T3			7.11	1.37	5.36	1.86	2.24	4.81
G4	7.69				5.59	2.49	2.62	4.95
G5	7.87				5.56	2.69	2.59	4.96
G6	7.74				6.03	2.60	2.76	4.93
T7			7.21	1.37	5.69	2.05	2.41	4.87
A8	8.25	7.56			6.22	2.65	2.85	5.00
C9			7.27	5.20	6.01	2.09	2.09	4.43
G10	7.89				5.92	2.59	2.73	4.79
T11			7.37	1.34	5.64	2.16	2.43	4.88
A12	8.21	7.42			6.14	2.64	2.79	5.00
C13			6.91	4.90	5.57	1.71	2.32	4.75
C15			7.20	5.10	5.42	1.81	2.21	
A16	8.30	7.66			6.24	2.71	2.89	5.01
T17			7.09	1.49	5.75	1.83	2.26	
G18	7.84				6.09	2.56	2.32	4.65
lesion	H2	H5	H7	H8	H1′	H2′	H2″	H3′
ϵA14	7.95	8.81	7.48	7.48	6.11	3.21	2.74	4.95

[a] 50 mM NaCl, 10 mM phosphate, D_2O, pH 6.8.

Table III: Proton–Proton Distance Constraints in the d(G4-G5-G6)·d(C13-ϵA14-C15) Segment of the ϵdA·dG 9-mer Duplex[e]

	intraresidue constraints on the same strand (Å)				
	base–H1′	base–H2′	base–H2″	H1′–H2′	H1′–H2″
G4	3.2–4.8[d]	2.1–3.2[c]	3.0–4.1[c]	2.5–3.6[c]	*a*
G5	*a*	2.1–3.2[c]	3.2–4.8[d]	*a*	*a*
G6	3.6–5.2[d]	2.1–3.2[c]	2.9–4.0[c]	2.4–3.5[c]	2.1–3.2[c]
C13	3.4–5.0[d]	2.0–3.1[c]	3.2–4.3[c]	2.7–3.8[c]	2.0–3.1[c]
ϵA14	2.0–3.1[c]	*b*	3.3–4.4[c]	2.9–4.1[d]	2.0–3.1[c]
C15	3.5–4.7[d]	2.1–3.2[c]	3.0–4.1[c]	*b*	2.1–3.2[c]
	interresidue constraints on the same strand (Å)				
	H1′–base	H2″–base	H2′–base	H6/H8–CH_3	H1′–CH_3
T3-G4	3.4–4.9[d]	2.7–3.8[c]	3.6–4.7[c]		
G4-G5	2.3–3.9[d]	2.1–3.4[d]	3.6–5.2[d]		
G5-G6	3.0–4.6[d]	nd	nd		
G6-T7	2.9–4.0[c]	2.3–3.4[c]	3.0–4.6[d]	3.0–4.6[d]	*b*
A12-C13	2.7–4.1[d]	2.3–3.1[c]	3.0–4.6[d]		
C13-ϵA14	*b*	*b*	*b*		
ϵA14-C15	*b*	*b*	*b*		
C15-A16	3.8–5.4[d]	2.7–3.8[c]	3.4–5.0[d]		
	base pair hydrogen-bonded distances (Å)				
	G4(O6)–C15(NH_2-4)			nr[f]	
	G4(NH1)–C15(N3)			1.6–2.2	
	G5(NH_2-2)–ϵA14(N1)			nr	
	G5(NH1)–ϵA14(N9)			nr	
	G6(O6)–C13(NH_2-4)			1.9–2.1	
	G6(NH1)–C13(N3)			1.9–2.1	

[a] Overlap. [b] Absent. [c] 50-ms data in D_2O. [d] 100-ms data in D_2O. [e] Base: H6 protons for pyrimidines, H8 protons for purines, and H2 proton for ϵA14. [f] nr, not restrained.

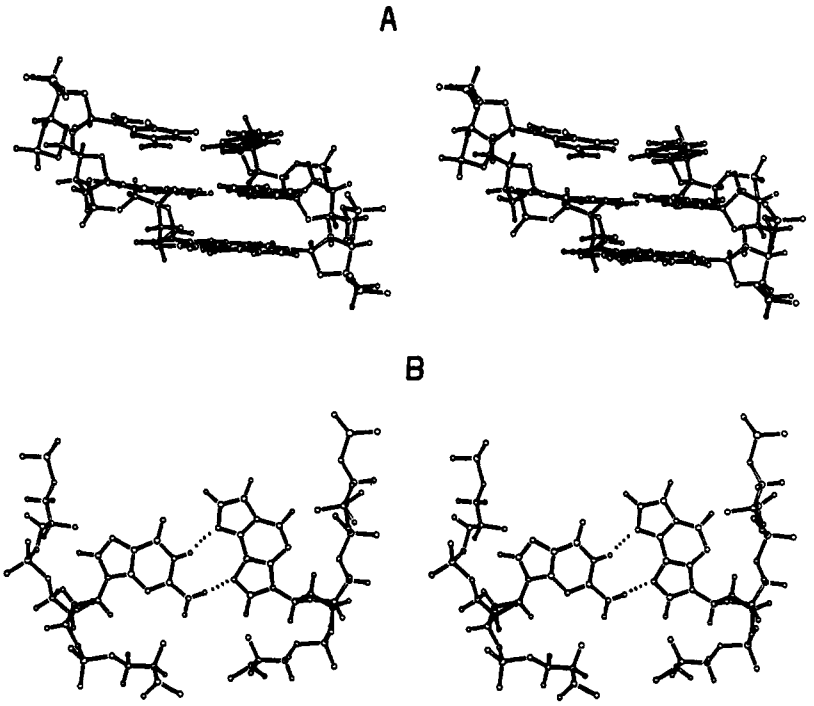

FIGURE 6: Stereopairs of (A) the d(G4-G5-G6)·d(C13-ϵA14-C15) trinucleotide segment viewed normal to the helix axis and (B) the dG5·ϵdA14 alignment viewed down the helix axis in the ϵdA·dG 9-mer duplex.

rapidly relieved during the first 30 steps of the energy minimization. Both starting structures converged to a similar energy-minimized structure. A stereoview of the energy-minimized structure for the central d(G4-G5-G6)·d(C13-ϵA14-C15) segment is shown in Figure 6A along with the alignment of the dG5·ϵdA14 base pairs as viewed down the helix axis (Figure 6B). The interproton distances for the central d(G4-G5-G6)·d(C13-ϵA14-C15) segment of the energy-minimized ϵdA·dG 9-mer duplex are tabulated in Table IV.

Discussion

General Structural Features of the Duplex. The thymidine imino proton chemical shifts (13.4–13.6 ppm) (Table I, Figure 1A) along with the observed NOEs to deoxyadenosine H2 protons within individual pairs (Figure 2A) establish Watson–Crick alignment of dA·dT pairs in the ϵdA·dG 9-mer duplex. Similarly, the deoxyguanosine imino proton shifts (12.2–12.7 ppm) (Table I, Figure 1B) are characteristic of imino protons hydrogen bonded to ring nitrogens such as occur in Watson–Crick dG·dC pairs. We are especially interested in the alignment at dG4·dC15 and dG6·dC13 pairs that flank the dG5·ϵdA14 lesion site in the ϵdA·dG 9-mer duplex. The observed NOEs between the imino proton of dG6 and the amino protons of dC13 (Figure 2A) are characteristic of Watson–Crick alignment for the dG6·dC13 pair. By contrast, the amino protons of dC15 are broad and preclude detection of the NOE characteristic of the dG6·dC13 alignment in the ϵdA·dG 9-mer duplex.

The ϵdA·dG 9-mer duplex is right-handed on either side of the dG5·ϵdA14 lesion site, based on the directionality of the observed NOEs between protons on adjacent base pairs along the duplex. These include NOEs between base protons and adjacent sugar (H1′, H2′,2″, H3′) protons in the 5′- but not the 3′-direction (Figures 4 and 5A), between adjacent base protons in purine H8/pyrimidine H6 (3′–5′) pyrimidine H5/CH_3 steps, and between deoxyadenosine H2 protons and sugar H1′ protons on the partner strand in the 3′-direction. Similarly, all glycosidic torsion angles at Watson–Crick dA·dT and dG·dC pairs adopt anti alignments in the ϵdA·dG 9-mer duplex, based on the very weak base to their own sugar H1′ NOEs in the short 50-ms mixing time NOESY spectrum of the ϵdA·dG 9-mer duplex (Figure S2B).

Table IV: Proton–Proton Distances in the d(G4-G5-G6)·d(C13-ϵA14-C15) Segment of the ϵdA·dG 9-mer Duplex from the Energy-Minimized Model[a]

	intraresidue distances on the same strand (Å)				
	base–H1′	base–H2′	base–H2″	H1′–H2′	H1′–H2″
G4	3.9	2.4	3.6	3.1	2.5
G5	3.9	2.3	3.6	3.1	2.5
G6	3.9	2.3	3.5	3.1	2.5
C13	3.8	2.2	3.3	3.1	2.5
ϵA14	2.6	4.6	4.1	3.1	2.5
C15	3.8	2.1	3.4	3.1	2.5

	interresidue distances on the same strand (Å)				
	H1′–base	H2″–base	H2′–base	H6/H8–CH_3	H1′–CH_3
T3-G4	3.3	2.7	4.3		
G4-G5	3.2	2.4	4.2		
G5-G6	3.5	3.7	5.0		
G6-T7	3.1	2.9	4.5	4.1	4.5
A12-C13	3.2	2.5	4.1		
C13-ϵA14	6.5	7.9	9.3		
ϵA14-C15	3.5	2.2	3.7		
C15-A16	3.0	2.5	4.3		

	intraresidue and interresidue distances on the same strand (Å)								
	C13			ϵA14			C15		
	H1′	H2′	H2″	H1′	H2′	H2″	H1′	H2′	H2″
ϵA14(H5)	3.1	3.9	2.2	6.2	3.9	5.4	8.8	8.2	9.4
ϵA14(H2)	6.5	9.3	7.9	2.6	4.6	4.1	3.5	4.4	5.2

	interresidue distances on partner strand (Å)				
	ϵA14(H5)	ϵA14(H8)	ϵA14(H7)	ϵA14(H2)	G5(NH1)
G4(NH1)	7.7	5.3	6.9	5.6	3.1
G5(NH1)	6.3	3.6	5.4	4.7	
G6(NH1)	5.6	4.7	5.4	4.9	3.6

[a] Base: H6 protons for pyrimidines, H8 protons for purines, and H2 proton for ϵA14.

ϵdA14(syn) Conformation. The NMR parameters definitively identify a syn glycosidic torsion angle at the ϵdA14 exocyclic adduct site in the ϵdA·dG 9-mer duplex. The strong

NOE between the H2 and sugar H1′ protons of ϵdA14 has an intensity comparable to the NOE between H6 and H5 protons of deoxycytidines (fixed separation of 2.45 Å) in the 50-ms mixing time NOESY spectrum of the ϵdA·dG 9-mer duplex (Figure S2B). The syn orientation at ϵdA14 is also reflected in the absence of NOEs between the H2 proton of ϵdA14 and the sugar H1′, H2′,2″, and H3′ protons of its 5′-flanking dC13 residue in the ϵdA·dG 9-mer duplex (Figures 4 and 5A). Further evidence consistent with a syn glycosidic torsion angle at ϵdA14 can be observed in the NOEs detected between the H5 proton of ϵdA14 and the H1′, H2′,2″, and H3′ protons of the 5′-flanking dC13 residue in the ϵdA·dG 9-mer duplex (Figures 4 and 5A).

dG5(anti) Conformation. We have assigned the 14.0 ppm exchangeable proton to the imino proton of dG5 on the basis of the observed NOEs between this proton and the imino protons of adjacent dG4 and dG6 in the one-dimensional NOE difference spectra of the ϵdA·dG 9-mer duplex (Figure 3B). These data establish that the imino proton of dG5 is directed into the helix consistent with an anti alignment and stacks with flanking dG4·dC15 and dG6·dC13 base pairs in the ϵdA·dG 9-mer duplex. Additional evidence supporting a dG5(anti) glycosidic torsion angle is the very weak observed NOE between the H8 and H1′ protons of dG5 in the 50-ms mixing time NOESY spectrum of the ϵdA·dG 9-mer duplex (Figure S2B).

dG5(anti)·ϵdA14(syn) Alignment. The 14.0 ppm resonance assigned to the imino proton of dG5 is to low field of the 12.2–12.6 ppm chemical shift range of deoxyguanosine imino protons involved in Watson–Crick dG·dC hydrogen bond formation. This observation establishes that the NH1 of dG5 forms a hydrogen bond with an acceptor ring N atom on ϵdA14 similar to the hydrogen bond between the NH1 of deoxyguanosines with the N3 of deoxycytidines in Watson–Crick dG·dC pairs. The additional downfield shift for the imino proton of dG5 in the dG5·ϵdA14 alignment must reflect the greater downfield in-plane ring current contribution of the ϵdA14 (three fused aromatic rings) compared to deoxycytidine. The ring nitrogens at positions N1 or N9 on the ϵdA14 ring are potential acceptors for the donor hydrogen bond from dG5 at the dG5(anti)·ϵdA14(syn) alignment site. We note that the imino proton of dG5 at the dG5·ϵdA14 lesion site exchanges much faster with increasing temperature compared to the imino protons of flanking dG4·dC15 and dG6·dC13 base pairs in the ϵdA·dG 9-mer duplex (Figure S1).

d(G4-G5-G6)·d(C13-ϵA14-C15) Segment. The interproton distances for the d(G4-G5-G6)·d(C13-ϵA14-C15) segment in the energy-minimized conformation (Table IV) may be compared with the input distance bounds (Table III) deduced from the volume integrals of the cross peaks in short mixing time NOESY spectra of the ϵdA·dG 9-mer duplex. The energy-minimized structure incorporates critical features of the experimental data for the trinucleotide segment centered about the lesion site. Specifically, adoption of the syn glycosidic torsion angle at ϵdA14 results in a 2.6-Å proton separation between the H2 and H1′ protons of ϵdA14, distances of <4 Å between the H5 proton of ϵdA14 and the H1′, H2′, and H2″ protons of dC13, and distances of >6 Å between the H2 proton of ϵdA14 and the H1′, H2′, and H2″ protons of dC13 in the energy-minimized structure (Table IV), consistent with the experimental constraints and NOE patterns (Table III; Figures 2–5). Further, the bases in an anti orientation stack over each other in the d(G4-G5-G6) segment such that the imino proton of dG5 is separated by <4 Å from the imino protons of flanking dG4 and dG6 in the energy-minimized structure (Table IV), consistent with the observed NOEs from the imino proton of dG5 to the imino protons of dG4 and dG6 in the ϵdA·dG 9-mer duplex (Figure 3). Further, the imino proton of dG5 is <4 Å from the H8 proton of ϵdA14 in the energy-minimized structure (Table IV), consistent with the NOE observed between the imino proton of dG5 and the superpositioned H7/H8 protons of ϵdA14 in the ϵdA·dG 9-mer duplex (Figure 3).

The dG5·ϵdA14 lesion site in the energy-minimized structure is stabilized by one hydrogen bond between the NH1 of dG5 and the N9 of ϵdA14 and a second hydrogen bond between the NH_2-2 of dG5 and the N1 of ϵdA14 (Figure 6B) as shown schematically in structure **3**. The flanking dG4·dC15 and

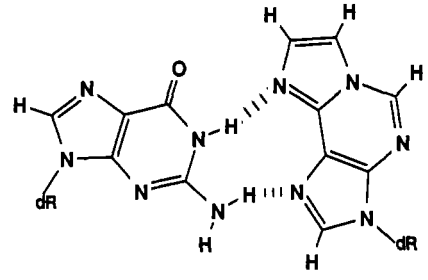

3

dG6·dC13 base pairs are intact and stack with the dG5·ϵdA14 pair in the ϵdA·dG 9-mer duplex. The stacking between dC13 and ϵdA14 is reflected in the upfield chemical shifts for the H6 (6.91 ppm) and H5 (4.90 ppm) protons of dC13 relative to other cytidines in the ϵdA·dG 9-mer duplex (Table II).

We comment below on some distances in the central d(G4-G5-G6)·d(C13-ϵA14-C15) segment of the energy-minimized structure that are in apparent conflict with the experimental data. An NOE should not be detected between the NH1 proton of dG4 and the H5 proton of ϵdA14 since the interproton distance is 7.7 Å in the energy-minimized structure with a dG5(anti)·ϵdA14(syn) alignment at the lesion site (Table IV). Experimentally, an NOE (peak N, Figure 2A) is detected in the 150-ms mixing time NOESY spectrum of the ϵdA·dG 9-mer duplex in H_2O solution at 2 °C. However, this NOE is absent in the NOESY data set recorded at 10 °C (Figure S3, supplementary material) and further cannot be detected in one-dimensional NOE difference spectra recorded at −8 °C (Figure S4, supplementary material). Thus, different data sets appear to be in conflict on this particular NOE, and no definitive conclusion can be drawn at the current time.

We experimentally detect weak NOEs between the H5 proton of ϵdA14 and the H2′ (peak A, Figure 5A) and H2″ (peak B, Figure 5A) protons of dC13 of approximately equal intensity in the 250-ms NOESY spectrum of the ϵdA·dG 9-mer duplex. By contrast, the energy-minimized structure predicts that the distance from the H5 proton of ϵdA14 to the H2″ proton of dC13 (2.2 Å) is much shorter than to the H2′ proton of dC13 (3.9 Å) (Table IV). This discrepancy may reflect inherent limitations associated with our attempts to generate pairing alignments based on a limited set of distance constraints defined by wide lower and upper bounds. Alternately, the discrepancy could reflect averaging between two or more pairing alignments at the dG5·ϵdA14 lesion site so that no single alignment could satisfy all the NMR-based distance constraints.

Motional Averaging of ϵdA14 Alignment. The base protons of ϵdA14 at the dG5·ϵdA14 lesion site and to a greater extent the base (H6, H5, and NH_2-4) protons of dC13 and dC15 at the flanking dG4·dC15 and dG6·dC13 base pairs are broad

in the ϵdA·dG 9-mer duplex. The increased line widths of base protons in the dC13-ϵdA14-dC15 segment are also reflected in either broad or weak NOE cross peaks involving these protons and other nearby protons in the ϵdA·dG 9-mer duplex. These data suggest that the observed broadening at the base protons of dC13 and dC15 probably monitors motional averaging among ϵdA14 alignments which occur on the intermediate NMR time scale.

Alignment of ϵdA14 opposite dT and dG. Our NMR studies establish that the alignment of the ϵdA exocyclic adduct in the interior of a DNA duplex depends on the base opposite it on the partner strand. Thus, in the previous paper we demonstrated that ϵdA adopts an anti orientation and the exocyclic ring is directed into the interior of the helix when positioned opposite thymidine, resulting in the ϵdA(anti) and dT(anti) base planes directed in opposite directions toward flanking dG·dC base pairs. By contrast, this paper demonstrates that ϵdA14 adopts a syn orientation and the exocyclic ring is directed toward the major groove when positioned opposite deoxyguanosine, resulting in a coplanar ϵdA(syn)·dG(anti) alignment stabilized by two hydrogen bonds (**3**).

Summary. The aim of the present study is to define the pairing alignment of ϵdA, a 1,N^2-exocyclic adduct of dA, with dG in the interior of a DNA duplex. Two-dimensional NMR studies establish that the potential steric clash between two purine bases, one of which has an additional exocyclic ring along its Watson–Crick pairing edge, is relieved through a dG5(anti)·ϵdA14(syn) alignment, **3**, stabilized by two potential hydrogen bonds. The exocyclic adduct is directed toward and is readily accommodated within the major groove when ϵdA14 adopts the syn orientation. This alignment positions the N1 and N9 atoms of ϵdA14 to serve as hydrogen bond acceptors from donor atoms of dG5(anti) positioned opposite it on the partner strand. The NH1 imino proton of dG5 at the lesion site resonates to low field at 14.0 ppm consistent with its participation in the hydrogen bonds that stabilize the dG5-(anti)·ϵdA14(syn) pairing alignment **3** at the lesion site. The observed broadening of the base but not sugar protons of dC13 and dC15 in the ϵdA·dG 9-mer duplex suggests conformational averaging among ϵdA14 alignments on the intermediate time scale, which would affect the stacking within the d(C13-ϵA14-C15) segment of the modified strand centered about the lesion site. The dG5(anti)·ϵdA14(syn) alignment **3** is readily accommodated into the DNA helix without disruption of flanking dG4·dC15 and dG6·dC13 base pairs and may account for the incorporation of dG opposite ϵdA during in vitro replication by DNA polymerase I.

Acknowledgments

NMR studies were undertaken on instruments purchased with funds provided by the Robert Woods Johnson, Jr., Charitable Trust and Matheson Foundation.

Supplementary Material Available

Figure S1, showing the exchangeable proton NMR spectra of the ϵdA·dG 9-mer duplex as a function of temperature, Figure S2, showing (A) the 250-ms mixing time NOESY contour plot of this duplex in D_2O and (B) an expanded contour plot of the 50-ms mixing time NOESY spectrum for this duplex, Figure S3, showing expanded contour plots of the 150-ms mixing time NOESY spectrum for this duplex in H_2O at 10 °C, and Figure S4, showing (A) the exchangeable proton NMR spectrum of this duplex at −8 °C and (B) the one-dimensional NOE difference spectrum following 0.5-s saturation of the G4 imino proton resonance (5 pages). Ordering information is given on any current masthead page.

References

Barbin, A., Bartsch, H., Leconte, P., & Radman, M. (1981) *Nucleic Acids Res. 9*, 375–387.

de los Santos, C., Rosen, M., & Patel, D. (1989) *Biochemistry 28*, 7282–7289.

Green, T., & Hathway, D. E. (1978) *Chem.-Biol. Interact. 22*, 211–224.

Hall, J. A., Saffhill, R., Green, T., & Hathaway, D. E. (1981) *Carcinogenesis 2*, 141–146.

Hare, D. R., Wemmer, D. E., Chou, S. H., Drobny, G., & Reid, B. R. (1983) *J. Mol. Biol. 171*, 319–336.

Kouchakdjian, M., Marinelli, E., Gao, X., Johnson, F., Grollman, A., & Patel, D. J. (1989) *Biochemistry 28*, 5647–5657.

Kouchakdjian, M., Eisenberg, M., Live, D., Marinelli, E., Grollman, A. P., & Patel, D. J. (1990) *Biochemistry 29*, 4456–4465.

Kouchakdjian, M., Eisenberg, M., Yarema, K., Basu, A., Essigmann, J., & Patel, D. J. (1991) *Biochemistry* (preceding paper in this issue).

Laib, R. J., & Bolt, H. M. (1977) *Toxicology 8*, 185–195.

Singer, B., & Bartsch, H. (1986) in *The Role of Cyclic Nucleic Acid Adducts in Carcinogenesis and Mutagenesis* (Singer, B., & Bartsch, H., Eds.) IARC Scientific Publications 70, pp 359–371, IARC, Lyon, France.

States, D. J., Haberkorn, R. A., & Ruben, D. J. (1982) *J. Magn. Reson. 48*, 286–292.